GEANT4 Emittance Diagnostics Simulations for the ERL Injector Prototype

Colwyn Gulliford
Physics Department, New College of Florida, Sarasota, Florida, 34243
(Dated: August 16, 2006)

The injector for the Energy Recovery Linac, a new high energy X-ray source under design at Cornell, will need to create ultra bright electron beams. One measure of this brightness, the transverse emittance, is the single most important characteristic of these beams. It is therefore crucial to be able get an accurate measure of this quantity. Two experimental designs to perform this measurement have been proposed and have been examined using computer simulation.

I. INTRODUCTION

GEANT4, a Monte Carlo simulation toolkit developed at CERN, was used to simulate two proposed emittance measurement experiments for the injector of the Energy Recovery Linac. In each design portions of the transverse phase space of an incoming beam were mapped out by passing the beam through either the combination of one slit and a scintillator or two precision slits and a faraday cup. From this mapping of phase space the standard deviation of the transverse divergence was calculated. Several design variables were tested in each set-up. These include slit material, scintillator and faraday cup response, as well as the geometry of various components and the relative distances between them. Simulations were also run to examine both scattering from and energy deposition in various experimental components.

II. BACKGROUND THEORY

When dealing with beam bunches of many particles it is not practical to calculate the individual particle trajectories. The use of phase space in conjunction with Liouville's theorem provides a useful tool for analyzing the collective characteristics of a beam as it moves along a beam line. The six dimensional phase space of a beam is a map of each particle's position and momentum coordinates (x, y, z, p_x, p_y, p_z). In linear beam dynamics coupling between the vertical and horizontal planes is not taken into account giving three independent two dimensional phase spaces: (x, p_x), (y, p_y), (z, p_z). It is customary to use the quantities x', y', and z' as opposed to p_x, p_y, p_z when the energy of the beam particles remains constant. Here x' is defined as the slope of the particles trajectory, dx/dz in the x-z plane and to first order is equal to the angle between the particles x and z momentum vectors.

Louville's theorem states that the density of particles in a beam's phase space remains constant when the beam particles are acted upon by conservative forces. This theorem is readily shown to hold in cases where the forces on the particles can be derived from macroscopic electric and magnetic fields [1]. For convenience particle beams are typically modeled as having an elliptical phase space portrait. The enclosed area of this phase ellipse is called the beam emittance and is given by

$$\epsilon_x = \sqrt{< x^2 >< x'^2 > - < xx' >^2} \tag{1}$$

Similarly, the normalized emittance, $\epsilon_{x,n}$, is defined as

$$\epsilon_{x,n} = \beta\gamma\sqrt{< x^2 >< x'^2 > - < xx' >^2} \tag{2}$$

The beams created in GEANT4 were generated by inputting the desired energy of the beam along with corresponding phase space parameters as shown in Table I. The values from the table were used to calculate the normalized momentum $\beta\gamma$, geometric emittance ϵ_x and the uncorrelated standard deviation of the transverse divergence $\sigma_{x'u}$.

$$\beta\gamma = \frac{\sqrt{E^2 - mc^2}}{mc^2} = \frac{p}{mc} \tag{3}$$

$$\epsilon_x = \frac{\epsilon_{x,n}}{\beta\gamma} \tag{4}$$

$$\sigma_{x'u} = \frac{\epsilon_x}{\sigma_x} \tag{5}$$

Both σ_x and $\sigma_{x'u}$ were entered into random gaussian distribution generators. The position values from this generator were then used to tilt the phase ellipse in phase space. This was accomplished by adding a linear term to the divergence values proportional to the position values. The constant of proportionality, α, is given below:

$$x' = x'_u + \alpha x \tag{6}$$

$$\alpha = \frac{\sqrt{\sigma^2_{x'} - \sigma^2_{x'u}}}{\sigma_x} \tag{7}$$

The values for both position and divergence were fed into the particle gun subroutine in GEANT4 and the beam was created. The recreation of the initial phase space of a 12.6 MeV beam is shown in Figure 1.

The values for both σ_x and $\sigma_{x'}$ were calculated from this plot. From the graph σ_x was determined to be 209 microns and $\sigma_{x'}$ to be 83.9 micro-radians. These values are to be compared with the input values for the 12.6 MeV beam given in Table I.

TABLE I: Input Beam Parameters.

Kinetic Energy (MeV)	0.3	0.5	0.75	12.6
$\epsilon_{x,n}$ (μm)	0.41	0.27	0.21	0.1
σ_x (mm)	2.29	1.26	0.64	0.21
$\sigma_{x'}$ (μrad)	1770	716	310	84

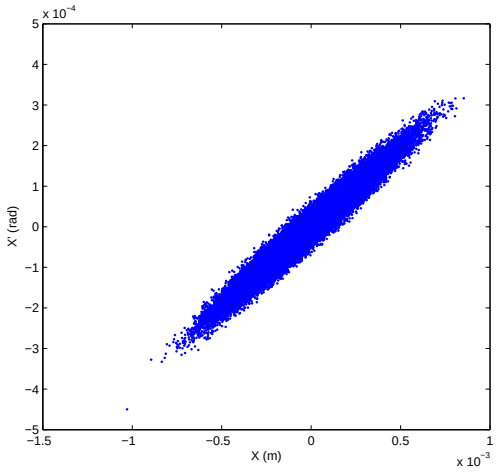

FIG. 1: Graph of Initial Phase Space for 12.6 MeV Beam (100k Electrons)

III. SINGLE SLIT FOLLOWED BY A CERIUM DOPED YTTRIUM ALUMINUM GARNET SCINTILLATOR (CE:YAG)

Before performing the actual slit experiment, the viability of the Ce:YAG scintillator had to be established. To do so a 2.5 x 2.5 mm Ce:YAG slab was created in GEANT4. The doping concentration in fraction mass of the yttrium aluminum garnert (YAG) was 0.18% cerium (Ce) to 98.12% YAG. The slab was broken into 5 x 5 micron bins in the x and y dimensions with each bin assigned to score energy deposition. A point sized beam of 100k electrons was fired along the z-axis and impinged upon the Ce:YAG slab at normal incidence in the x-y plane. Simulations were run with beam kinetic energies of 0.3, 0.5, 1, 5, and 15 MeV. Energy deposition was handled by the G4VPrimitive Scoring G4PSEnergyDeposit concrete class in GEANT4. At each beam energy runs were produced for a slab thickness of 50, 100, 250, 500 microns. The standard deviation of the spot size was calculated from the energy distribution along the x-axis at each data point. The nonzero spot size seen in these simulations is caused by multiple scattering of secondary electrons and gammas in the Ce:YAG slab. The full width at half maximum was estimated for the 0.5 MeV runs. It should be noted that the energy distribution functions were highly non-gaussian making for an exact measurement of the full width at half maximum a more challenging exercise.

The results suggest that a Ce:YAG scintillator with a thickness of 100 microns will work for higher energies (15 MeV). For lower energies (0.5 MeV) 50 microns will work, however material this thin is both more expensive and harder to work with.

Building on these results, one slit emittance simulations with 100 micron scintillator thickness were run using both copper and tungsten slits at high energy (12.6 MeV). In these simulations several design parameters were varied. These include the slit thickness, the distance from the slit to scintillator, and for select runs the thickness of the scintillator. Figure 3 shows the basic geometry of these simulations.

The mapping of phase space in this experiment is accomplished by passing the beam through a small slit. This selects out a portion of phase space along the transverse axis. The distribution of beam particles along the transverse axis is measured by the spread in energy deposition in the Ce:YAG slab. To first order the transverse position of a particle at

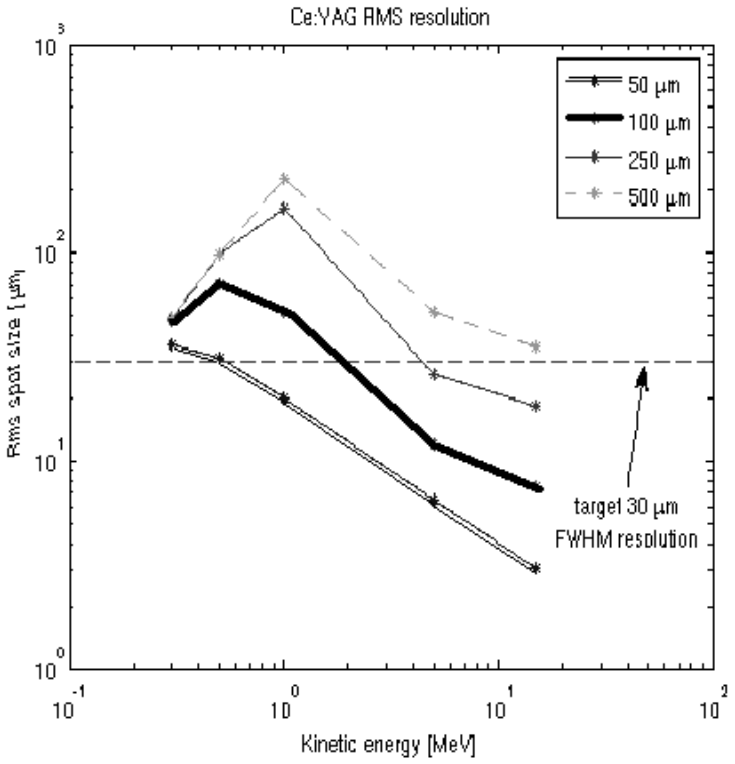

FIG. 2: RMS values of the spot size on the Ce:YAG slab calculated from deposited energy distribution recorded by GEANT4 for several beam energies and slab thicknesses

the scintillator is equal to the drift distance between the slit and the slab times the particle's divergence. This allows for the calculation of the rms value of the uncorrelated divergence, $\sigma_{x'u}$ by dividing the rms value of the transverse position spread of the beam on the slab by the distance to the YAG screen. Scanning the slit in the transverse direction would then allow for the entire phase space to be mapped out by finding the spread in divergence at every transverse position of the phase ellipse. As before energy deposition was handled by the G4PSEnergyDeposit concrete class in GEANT4. In these simulations several design parameters were varied. These include the slit thickness, and the distance from the slit to screen, see Figure 4.

The results for copper show that for a slit thickness of 4 mm or more there is only a slight dependence on the thickness and the error in the $\sigma_{x'u}$ measurement. Not shown in these graphs are the results for the 2 mm thick slit. The error in the $\sigma_{x'u}$ measurement for these runs varied from 20% to 100%.

The results for tungsten demonstrate a stronger trend between the slit thickness and the error in the measurement of $\sigma_{x'u}$. These results also demonstrate that a 2 mm thick slit yields good results.

After running these simulations and finding that the measured values for $\sigma_{x'u}$ were consistently smaller than the input or expected value, runs were set up with 200 and 300 micron Ce:YAG slab thickness. The results for both copper and tungsten are shown in Figure 7 and 8 respectively.

Low energy simulations were also carried out. The beam energy for these runs was 0.5

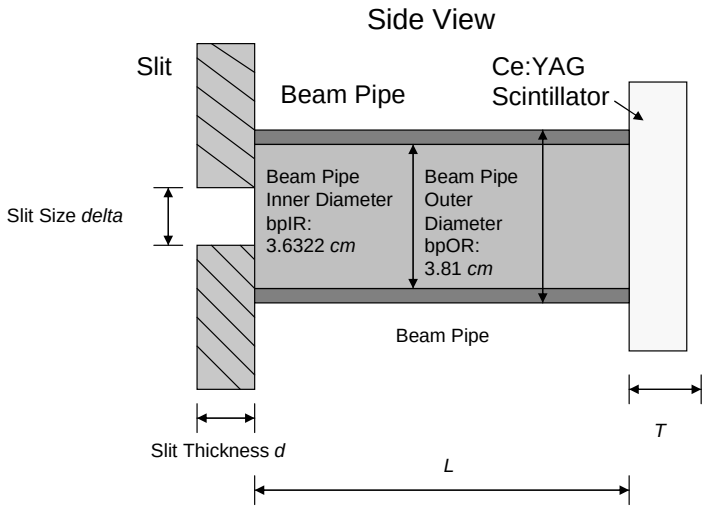

FIG. 3: One Slit with Ce:YAG Scintillator Simulation Set-up

Kinetic Energy = 12.6 *MeV*
Distance to Screen *L* = 1.5, 2.0, 2.5, 3.0 *m*
Slit Material : Copper and Tungsten
Slit Size *delta* = 10 microns
Slit Thickness *d* = 2.0, 4.0, 6.0, 8.0, 10 *mm*
Ce:YAG Thickness *T* = 100, 200*, 300* microns
Number of Electrons: 5e6
These values were used based on data from space charge simulations

FIG. 4: Run parameters for high energy one slit simulation [2].

MeV. All runs were carried out with 100 micron thick Ce:YAG. The results for these runs were not as accurate as the ones for high energy, as shown in Table II.

IV. 2 SLITS WITH FARADAY CUP

The second experimental design calls for two high precisions slits in conjunction with a faraday cup. In this set-up the beam is first passed through an armor slit. This piece of equipment is designed to absorb a large amount of the beam energy before it reaches the high precision slits. This is done so that the energy impinging on the precision slits is not substantial enough to cause deformation of the slit material due to heat. Once the beam has passed the armor slit, it is run through a series of two high precision slits. The first of these slits is used to select out a portion of the beam's phase space along the transverse axis as was done in the one slit experimental design. Next, the beam passes through a second high precision slit. This selects out particles with a specific divergence. The number of particles that make it through both slits are then counted using a faraday cup. This is a cylinder of copper with a cone shape cut out in the front to accept electrons coming from the slit

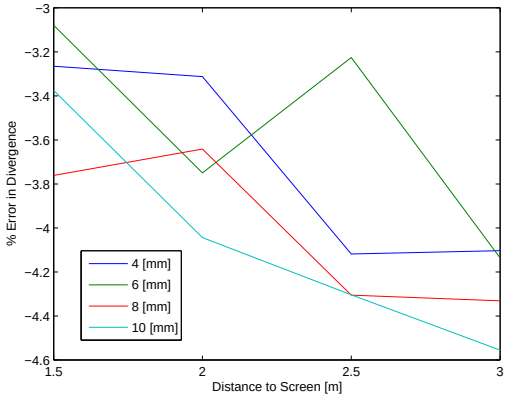

FIG. 5: Graph of Percent Error in the Measurement of $\sigma_{x'u}$ vs. Distance to the Ce:YAG Screen for several copper slit thicknesses. At this energy the input $\sigma_{x'u} = 19.33$ μrad

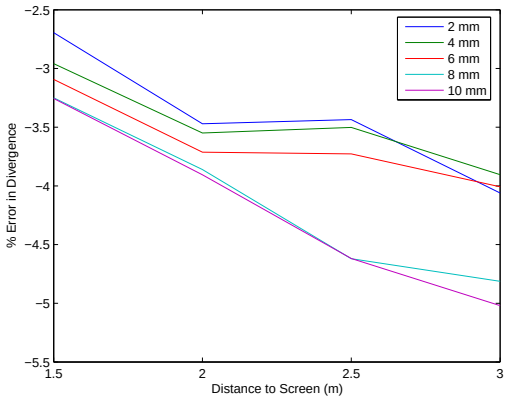

FIG. 6: Graph of Percent Error in the Measurement of $\sigma_{x'u}$ vs. Distance to the Ce:YAG Screen for several tungsten slit thicknesses. At this energy the input $\sigma_{x'u} = 19.33$ μrad

arrangement. The number of electrons deposited is calculated from the current measured off the faraday cup. In order to get a $\sigma_{x'u}$ measurement the second slit is scanned to allow particles of all divergences to pass through both slits. The number of particles at each position gives rise to a position distribution which then can be used as before to calculate the $\sigma_{x'u}$ value. To make a full emittance measurement, both slits would be scanned in order to map out the entire phase space of the beam.

Two designs were used in simulations for this experimental set-up: one for high energy and one for low energy. In both cases several other measurements were taken to explore other important characteristics of each design. These measurements include for both high and low energy geometries: back scattering from the armor slit, energy deposition on all three slits, and the signal to noise ratio of the each set-up. For low energy, back scattering of electrons from the faraday cup was also explored. It should be noted that after running the signal to noise ratio simulations for low energy it was decided to add in a 'beam stop' at the position of the second precision slit in both geometries. This beam stop is made of a large piece of copper or tungsten (for low and high energy respectively) with a section cut out to allow particles to reach the second precision slit. The inclusion of this piece resulted

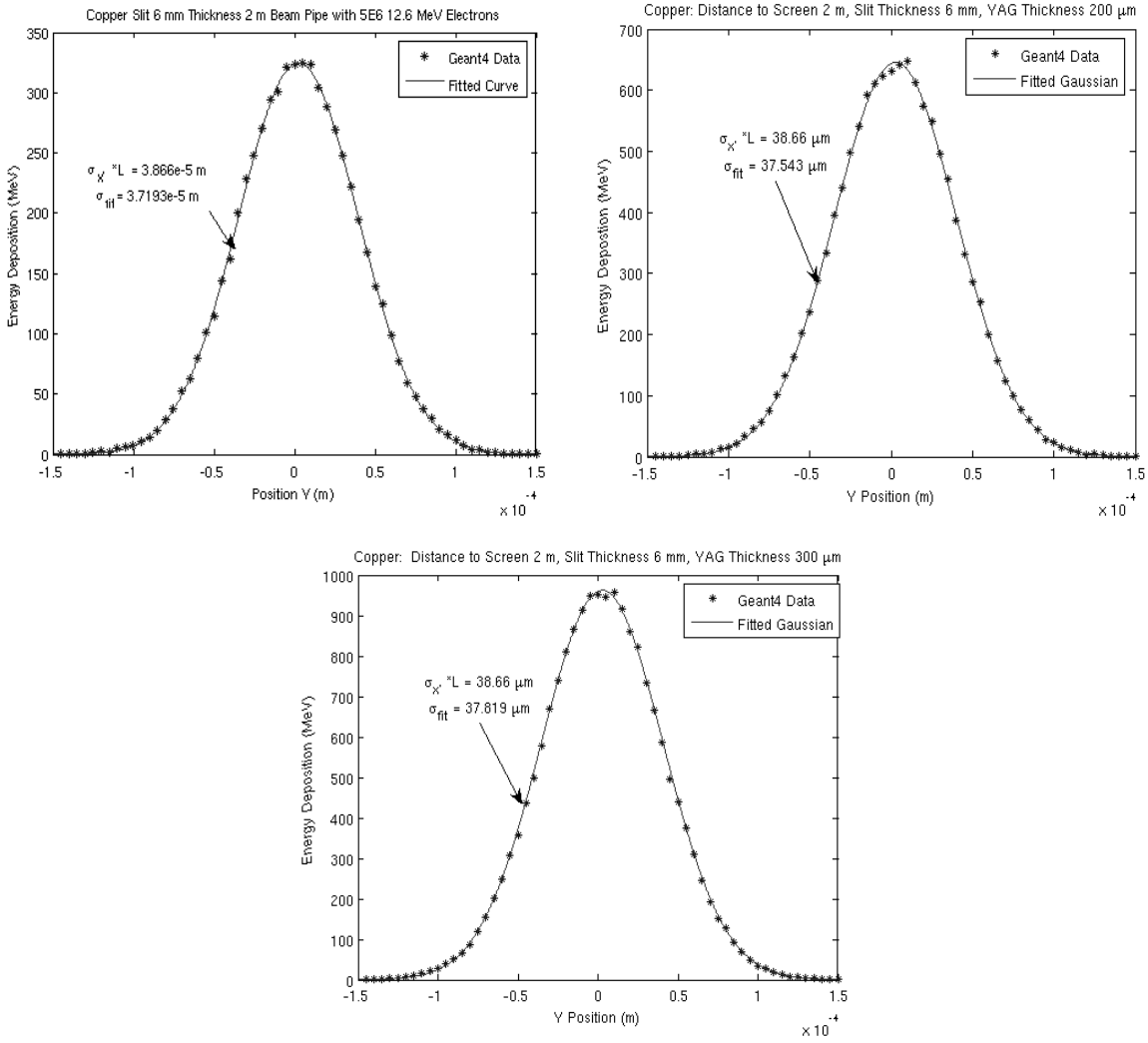

FIG. 7: Position spread of 12.6 MeV beam at Ce:YAG scintillator for 100, 200, 300 μm Ce:YAG thicknesses (from top left to right and down) for a 6 mm copper slit 2 m from the slab. The error in the calculations of $\sigma_{x'u}$ are -3.8%, -2.9%, and -2.7% respectively.

in much higher signal to noise ratios. The geometries of the beam stops are displayed in Figure 14 and 16 in the appendix.

Shown in Figures 14 and 15 in the appendix is the low energy geometry and layout for the 2 slit experiment.

The first simulations run for the two slit experimental set-up were used to examine the amount of back scattering off the armor slit. In these runs a cylindrical beam of uniform distribution and width of 0.3 mm width was fired into the armor slit. The beam was offset by 0.5 mm allowing for most of the impacting electrons to strike the armor slit just above the position of the opening. Two beam energies were tested, 0.5 MeV and 12.6 MeV. For the 0.5 MeV beam the armor slit was made of copper, for the 12.6 MeV beam the slit was made of tungsten. The full angle of the large opening of the armor slit was varied from 10 to 90 degrees. Each run consisted of 10k electrons. It should be noted that the geometry of the armor slit used in these simulations is that of the low energy geometry. For low energy

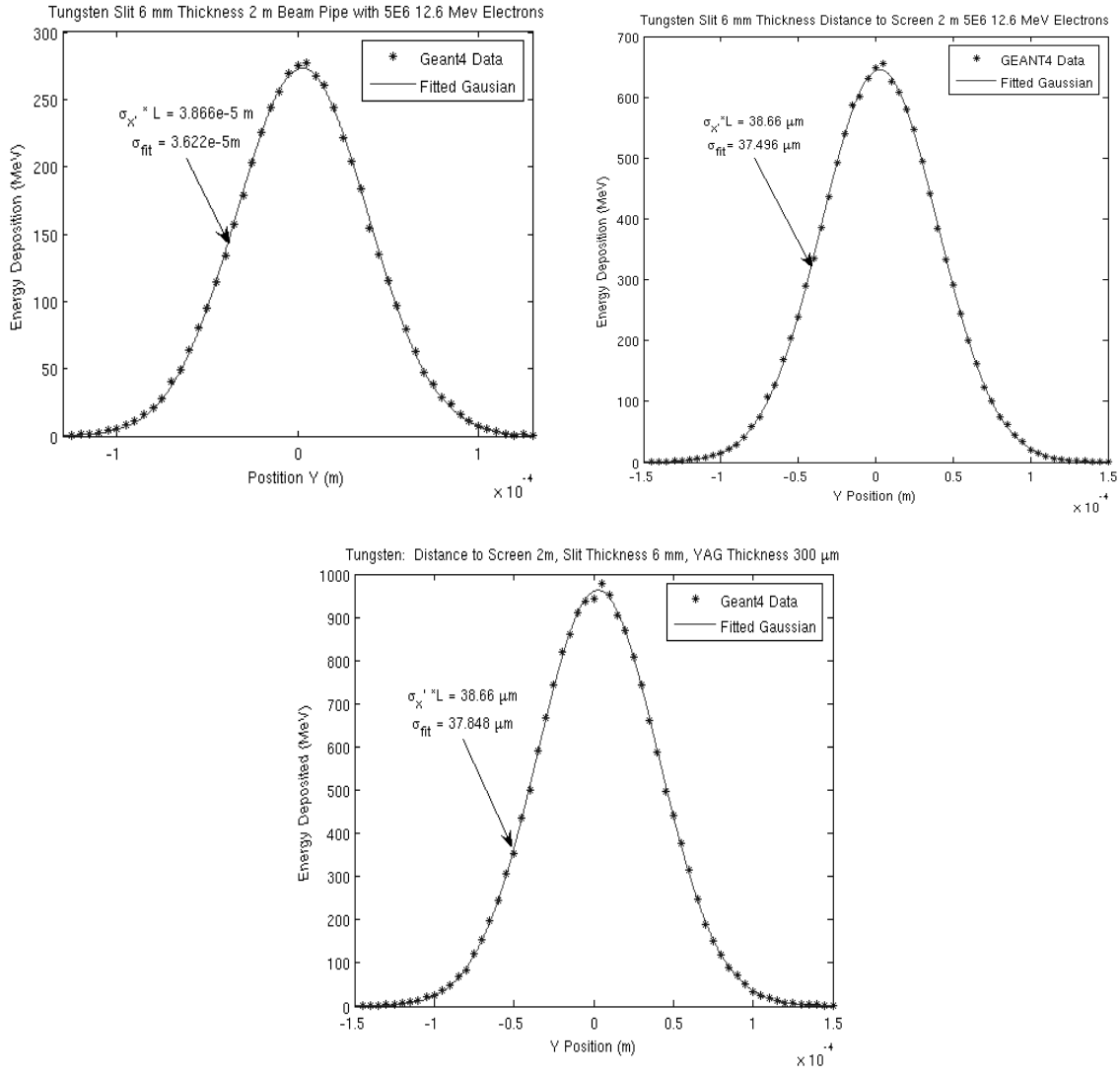

FIG. 8: Position spread of 12.6 MeV beam at Ce:YAG scintillator for 100, 200, 300 μm Ce:YAG thicknesses (from top left to right and down) for a 6 mm Tungsten slit 2 m from the slab. The error in the calculations of $\sigma_{x'u}$ are -6.3%, -3.1%, and -2.1% respectively.

the percentage of back scattered energy from the slit varies from about 1% at 10 degrees to about 7% at 90 degrees. For high energy the results show a similar pattern, however the values here range from about 0.1% at 10 degrees to about 0.6% at 90 degrees and are shown in Figure 9.

The next set of simulations explored the effects of electrons back scattering out of the faraday cup. The first set of runs consisted of firing a point beam along the z axis offset from the center of the cup. Two offsets, 1 mm and 5 mm, were simulated. The full opening angle of the faraday cup was then scanned from 10 to 50 degrees in 10 degree intervals. The results of these scans are given in Figure 10

From this data two simulations, one for a 20 degree faraday cup opening and the other for a 30 degree opening, were set up to test the amount of back scattering from the cup while the beam is scanned in the transverse direction. Figure 11 shows the results for both

TABLE II: Results for low energy (0.5 MeV) single slit experiment

Run Number	$\sigma_{x'u}$ (in 10^{-4} rad)	Percent Error from accepted value of 1.255E-4 rad
1	1.7136	36.5
2	1.8983	51.3
3	1.6925	34.9
4	1.5337	22.2
5	1.6292	29.8
6	1.6279	29.7
7	1.58	25.9
8	1.6247	29.4
9	1.8876	50.4
10	1.5176	20.9

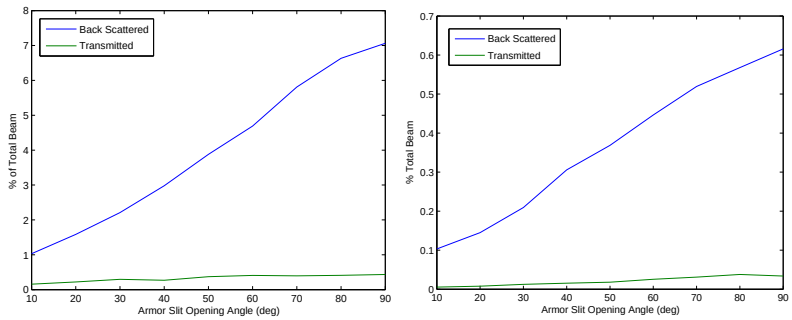

FIG. 9: On the left: Back Scattering of a 0.5 MeV Beam vs. Armor Slit Opening Angle. On the right: Back Scattering of a 12.6 MeV Beam vs. Armor Slit Opening Angle.

20 and 30 degree opening angles.

The final simulations for the low energy two slit experimental set-up consisted of a signal to noise ratio measurement and a slit scan $\sigma_{x'u}$ measurement. The signal to noise ratio calculation was carried out by first aligning the precision slits with zero transverse displacement and firing a 0.75 MeV beam through the set-up to the faraday cup. The amount of charge deposited on the faraday cup in electron counts was used as the signal measurement. Next the second precision slit and beam stop were displaced along the transverse axis so as to completely block any incoming particles. A 0.75 MeV beam was again shot and the charge deposited in electron counts on the faraday cup was measured and taken as the noise signal. With the beam stop included in the simulation geometry no noise signal was measured. After confirming that the design had a large signal to noise ratio, a scan of the second slit was simulated. For this run the second precision slit was scanned from -4σ_{x0} to 4σ_{x0} in steps of σ_{x0}. Here σ_{x0} is the expected rms value of the position spread of the beam at the second slit and is equal to the initial $\sigma_{x'u}$ value times the drift distance between the first and second slit. The beams for this scan consisted of one million electrons at 0.75 Mev. Figure 12 shows the GEANT4 data along with the with a fitted gaussian curve. The expected value for σ_{x0} was 55.3 microns. The value obtained from the fitted gaussian was 55.2 microns, giving an error of -0.18%. Both the signal to noise ratio and the precision slit scan simulations used an initial position filter of the same size as the armor slit aperture (0.008"). The filter consisted of only firing particles with initial transverse position values within the range of the armor

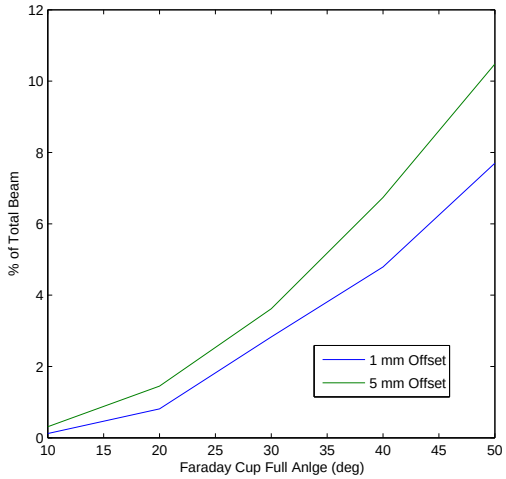

FIG. 10: % of 10k Incoming Electrons Back Scattered out of the Faraday Cup vs. Faraday Cup Opening Angle for 1 mm and 5 mm transverse beam offsets

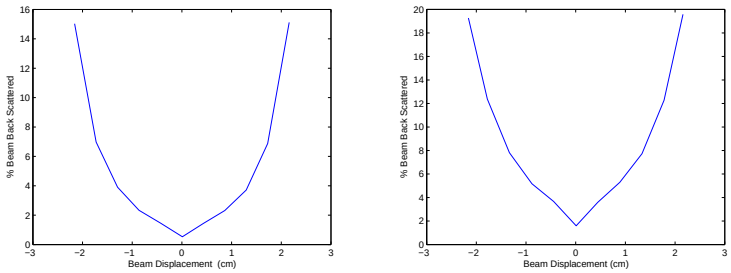

FIG. 11: On the left: % of Incoming Electrons Back Scattered from the Faraday Cup vs. Transverse Position of 0.5 MeV Point Source Beam for Faraday Cup with 20 degree Opening Angle. On the right: % of Incoming Electrons Back Scattered from the Faraday Cup vs. Transverse Position of 0.5 MeV Point Source Beam for Faraday Cup with 30 degree Opening Angle.

slit aperture and was used to cut down on simulation run time.

The high energy geometry for the two slit experimental set-up was based off the low energy geometry and has only a few minor changes. Figures 16 and 17 display the dimensions and layout of the experimental equipment for this simulation. Differences between this and the low energy design include the use of a tungsten-copper alloy for the three slits and beam stop materials, a change in the dimensions of the armor slit and faraday cup, and a change in the design of the precision slits as well as the method of mounting them in the beam stop. The tungsten-copper alloy had a fractional weight ratio of 90% tungsten to 10% copper. As with the low energy design both a signal to noise measurement and slit scan $\sigma_{x'u}$ measurement were carried out. For the signal to noise measurement twenty runs of 10k electrons were performed with all three slits aligned on the z-axis. This gave an average signal value of 88.5 electron counts deposited in the faraday cup. The same number of runs were processed with the second precision slit and beam stop offset along the transverse axis blocking the beam. These runs resulted in a noise value of -1/20 electron counts. This gives a signal to noise ratio of -1770. Upon confirming that the set-up had a large enough signal to noise

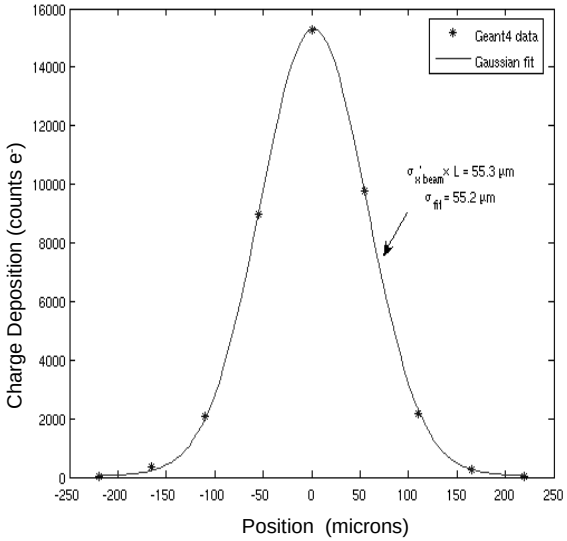

FIG. 12: Graph of position spread of a 0.75 MeV Beam at the second precision slit. The distance between the first and second slit was 38 *cm*. At this energy the input $\sigma_{x'u}$ = 145.6 μrad and $\sigma_{x'u}L$ = 55.3 μm. The rms value of the fitted curve σ_{fit} = 55.2 μm, giving a % error of -0.18 in the measurement.

ratio, a slit scan $\sigma_{x'u}$ measurement was simulated. For this simulation the second precision slit was scanned from -3.5σ_{x0} to 3.5σ_{x0} in steps of $\sigma_{x0}/2$. Again σ_{x0} is the rms value of the expected position spread of the beam particles at the second precision slit and is equal to the input $\sigma_{x'u}$ value times the drift distance between the two precision slits. For the high energy set-up with a 12.6 MeV beam σ_{x0} is 25.129 microns. Figure 13 shows the charge deposition on the faraday cup vs. position of the second slit. A gaussian fit was applied to this data and the rms value of this fit was measured to be 24.437 microns. This gives an error of -2.75% with respect to σ_{x0}.

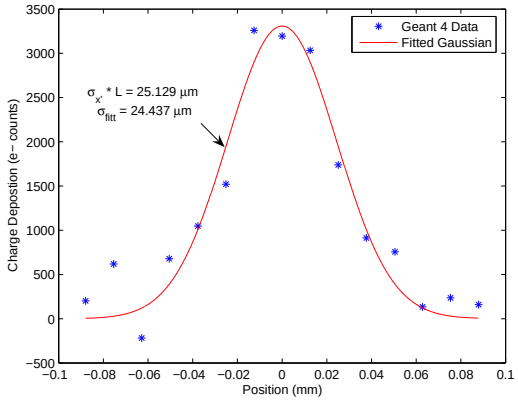

FIG. 13: Graph of position spread of a 12.6 MeV Beam at the second precision slit. The distance between the first and second slit was 1.3 *m*. At this energy the input $\sigma_{x'u}$ = 19.33 μrad and $\sigma_{x'u}L$ = 25.129 μm. The rms value of the fitted curve σ_{fit} = 24.437 μm, giving a % error of -2.75 in the measurement.

The final simulation run for the two slit experiment design was to record energy deposition in all three slits and in the beam stop for both high and low energies. In both cases all three slits were aligned along the z-axis. The beam energies were the same as for the high and low energy slit scans: 0.75 and 12.6 MeV. Ten thousand electrons were fired in both runs and the energy deposited in slits and beam stop recorded. Table III displays these values.

TABLE III: Percentage of the Total Beam Energy Absorbed (10k Electron Beam)

Beam Energy MeV	0.75	12.6
Armor Slit	91%	48%
Precision Slit 1	5.7%	20%
Precision Slit 2	0.57%	0.80%
Beam Stop	0%	0.2%
Armor Slit Opening	200 μm	80 μm

These results show that the armor slit is performing its function well at low energy, absorbing 90% of the total beam energy. In this case the first precision slit is not absorbing a large amount of the total beam energy. This is different for the 12.6 MeV beam, where the armor slit only absorbs 48% of the total beam energy and the first precision slit receives 20% of the total beam energy. This value is higher than desired.

V. RESULTS AND CONCLUSIONS

For the one slit with Ce:YAG scintillator set-up the GEANT4 data suggests that for high energy (12.6 MeV in simulation) accurate measurements of the position spread of the beam and thus the rms value of the uncorrelated divergence spread can be achieved. Accurate measurements were carried out using 100, 200, and 300 micron Ce:YAG slab thickness. For these runs the distance from slit to scintillator was 2 m and the slit thickness 6 mm. The percent errors in the calculation of $\sigma_{x'u}$ for these runs were -3.8%, -2.9%, and -2.7% for the slab thicknesses respectively. It should be noted that the values retrieved from the simulations are consistently lower than the input value. One possible explanation for this is that a significant number of beam particles were seen to scatter off the inside surfaces of the slit, and thus have the opposite value of divergence. If these results are physical then it could be expected that a compensating effect due to space charge interaction will make for more accurate measurements. With this in mind the realistic error expected in these measurements is roughly 5 to 10%. The low energy simulations for this set-up yielded errors in the calculation of $\sigma_{x'u}$ that ranged from roughly 20 to 50%, demonstrating that this experimental set-up is not viable at lower energies.

In the case of the two slit with faraday cup simulations showed that the amount of energy back scattering off the armor slit at both 0.5 and 12.6 MeV was within acceptable limits ($<$ 10% of the total input beam energy) for the proposed armor slit opening of 90 degrees. At 0.5 MeV the back scattering of electrons out of the faraday cup was simulated and shown to be within acceptable limits for both 20 and 30 degree faraday cup openings. Signal to noise ratio measurements were simulated for both the high and low energy two slit experimental designs with beam energies of 0.75 MeV and 12.6 MeV respectively. For the low energy geometry no noise was recorded. For the high energy geometry an average signal

over twenty simulations was calculated to be 88.5 electron charges deposited on the faraday cup. Averaging over twenty runs with the beam blocked by the second slit and beam stop, the noise value was calculated to be -1/20, giving a signal to noise ratio of -1770. These runs confirmed that the signal to noise ratios for both the high and low energy geometries was within acceptable values (absolute value of the ratio > 1000). Measurements of $\sigma_{x'u}$ were simulated for both a 0.75 MeV and 12.6 MeV beam by scanning the second precision slit. In the lower energy run the slit was scanned from -4σ_{x0} to 4σ_{x0} in steps of σ_{x0} where σ_{x0} is the expected rms value of the position spread of the beam at the second precision slit. For the 0.75 MeV beam $\sigma_{x0} = 55.3\mu$m. The slit scan was simulated and a value for σ_{x0} calculated from the data to be 55.2 μm giving an error of -0.18%. A similar simulation was run for the high energy geometry. In this simulation, the second precision slit was scanned from -3.5σ_{x0} to 3.5σ_{x0} in steps of $\sigma_{x0}/2$. At this energy, 12.6 MeV, $\sigma_{x0} = 25.129\mu$m. The value for σ_{x0} calculated from the GEANT4 data was 24.437μm, giving an error of -2.75%. These results demonstrate that the two slit experimental set-up should yield accurate results for both high and low energy beams (as simulated with respective geometries and beam stops in place).

Future work for this project includes simulations for neutron production in the beam dump of the ERL injector are needed in order to get an understanding of the amount of shielding that will be required around the beam line and beam dump.

VI. ACKNOWLEDGMENTS

I would like to thank Dr. Ivan Bazarov, of Cornell University, who proposed this Research Experience for Undergraduates project and guided my efforts throughout the course of this project. This work was supported by the National Science Foundation REU grant PHY-0552386 and research co-opertaive agreement PHY-9809799.

---

[1] H. Wiedmann *Particle Accelerator Physics: Basic Principles and Linear Beam Dynamics* **77**, 123 Springer-Verlag (1993).

[2] I. Bazarov *Slits and Peppers*

VII. APPENDIX: TWO SLIT GEOMETRY AND LAYOUT SPECIFICATIONS

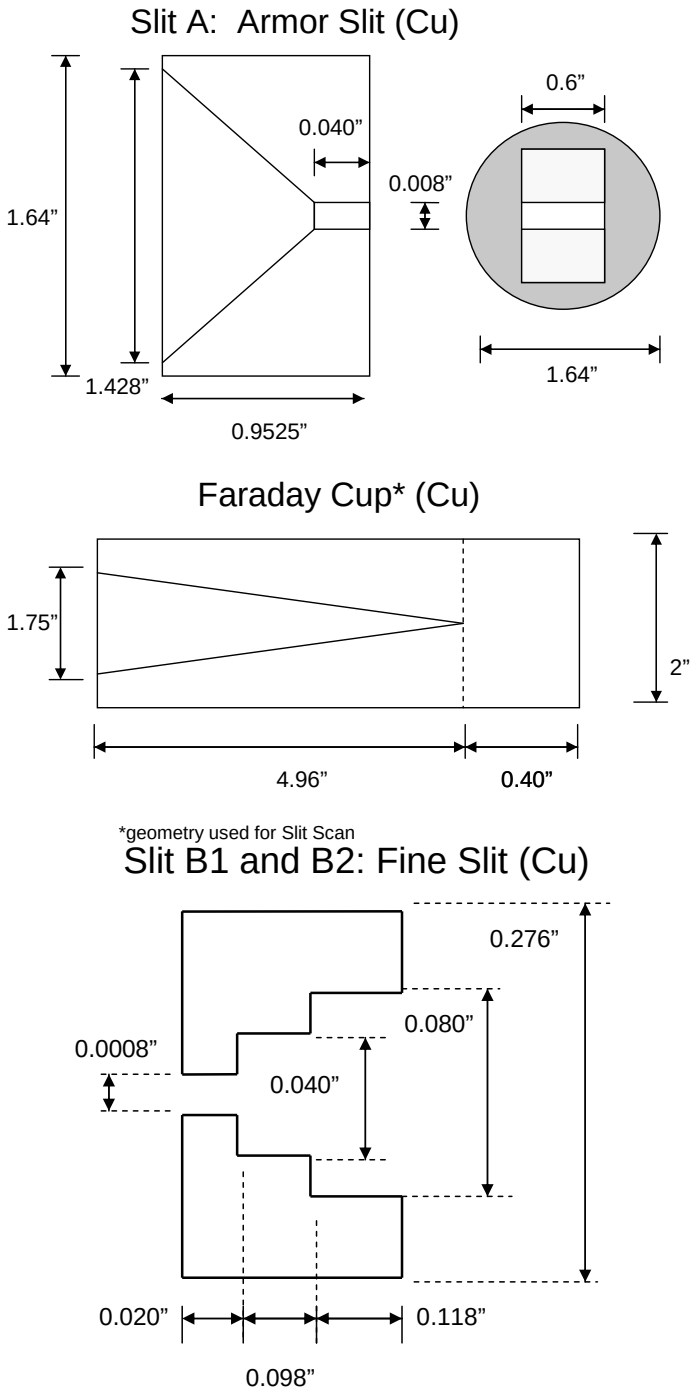

FIG. 14: Low Energy Slit Simulation Geometry

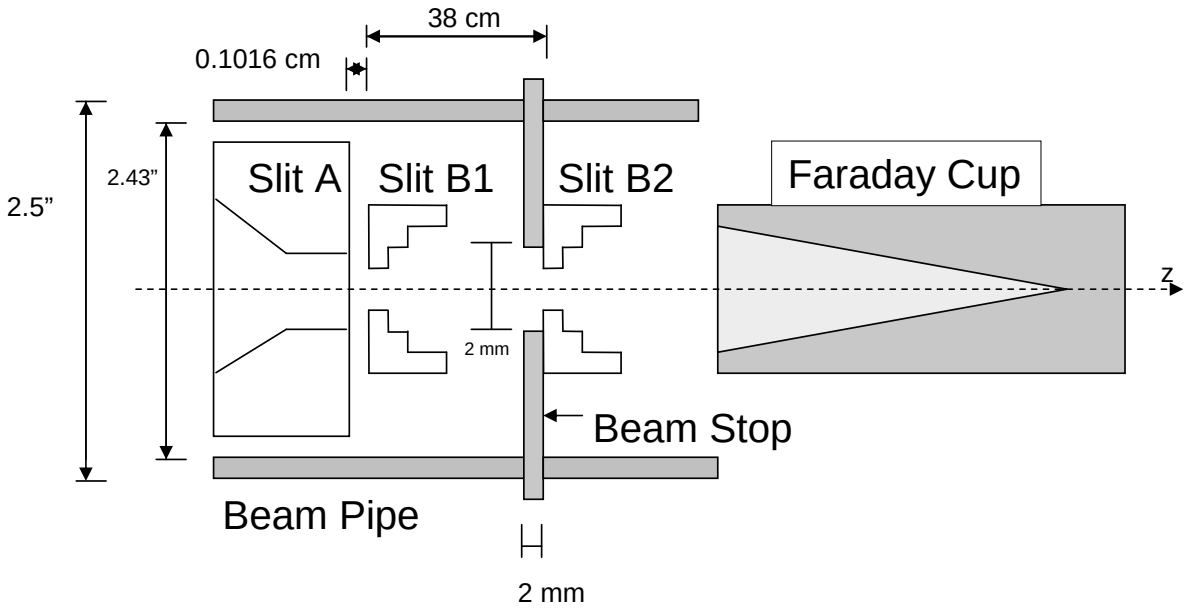

FIG. 15: Low Energy Two Slit Simulation Layout

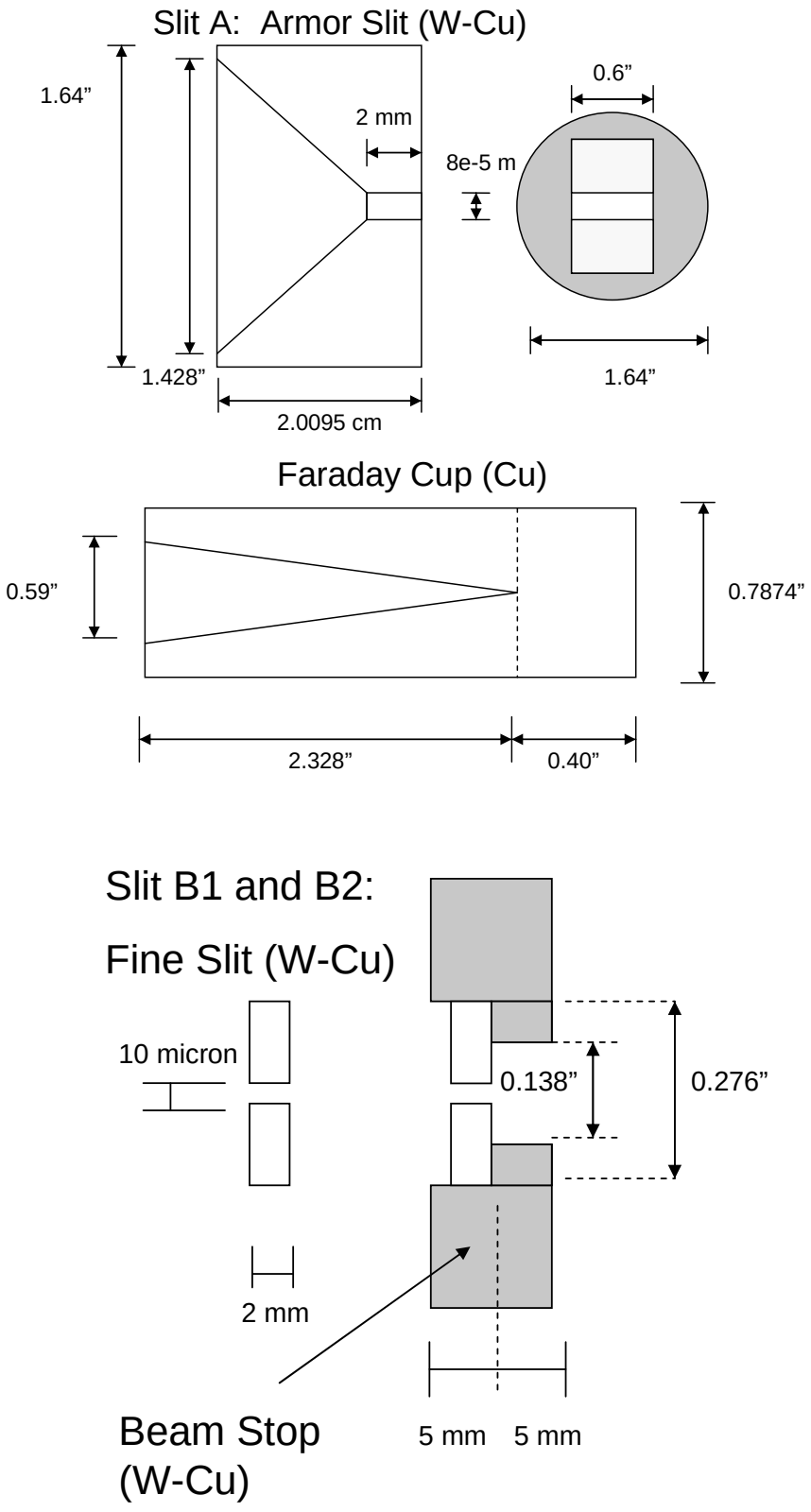

FIG. 16: High Energy Two Slit Simulation Geometry

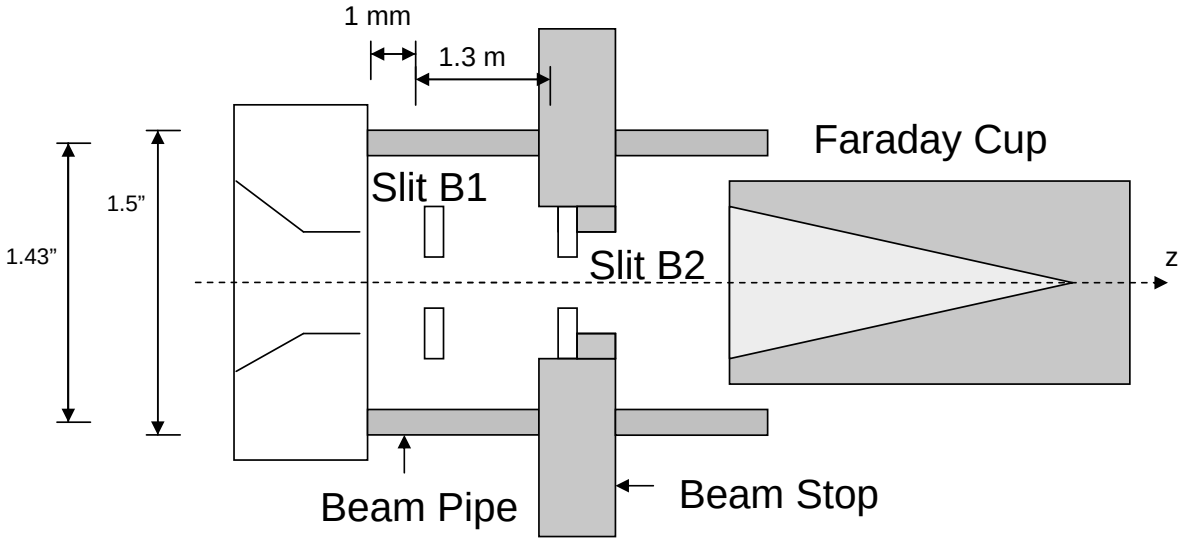

FIG. 17: High Energy Two Slit Simulation Layout